JOURNAL OF GEOPHYSICAL RESEARCH, VOL. 104, NO. A3, PAGES 4399-4410, MARCH 1, 1999

Auroral density fluctuations on dispersive field line resonances

R. Rankin, J. C. Samson, V. T. Tikhonchuk[1] and I. Voronkov

Department of Physics, University of Alberta, Edmonton, Canada

Abstract. A model is presented that describes the excitation of density perturbations and parallel electric fields by standing shear Alfvén waves on dipole fields in Earth's magnetosphere. The model includes the effects of electron inertia and gyro-kinetic dispersion, accounting for field-aligned variations of the electron and ion temperatures and the ambient plasma density. In a model dipole magnetosphere, it is found that dispersion and nonlinearity determine the depth, spatial structure, and temporal evolution of large-amplitude density fluctuations near to the polar ionospheres. The characteristics of magnetospheric density cavities and their relationship to auroral luminosity, or field-aligned currents, is discussed in the context of recent satellite and ground based observations.

1. Introduction

Density cavities are a common feature in the topside auroral ionosphere and magnetosphere and are often seen at altitudes ranging from 1500 km [*Lundin et al.,* 1994; *Stasiewicz et al.,* 1997] to greater than 4 Earth radii 4 R_E [*Persoon et al.,* 1988]. Perpendicular scale sizes vary from a number of kilometers (several electron inertia lengths λ_e in the auroral accelerator region) [*Stasiewicz et al.,* 1997] to many tens of kilometers [*Persoon et al.,* 1988]. Their origin is unknown, but observations indicate that density cavities are often associated with the auroral acceleration process [*Lundin et al.,* 1994; *Persoon et al.,* 1988; *Stasiewicz et al.,* 1997]. Consequently, theories that describe particle acceleration into the ionosphere, and the associated structure of auroral luminosity, must account for processes that produce magnetospheric density fluctuations and explain the relationships that exist between all these phenomena.

Recent observations, computer models, and theory [*Samson et al.,* 1996; *Streltsov and Lotko,* 1997; *Trondson et al.,* 1997; *Wei et al.,* 1994] have suggested that ULF, shear Alfvén field line resonances (FLRs) can produce certain types of auroral arcs. FLRs can have overall latitudinal scale sizes of tens of kilometers in the polar ionosphere [*Samson et al.,* 1996] that are comparable to the perpendicular scale of density cavities. Mode conversion to electron inertia and/or ion kinetic waves within FLRs can lead to even smaller structures, on the scale of a number of kilometers in the auroral ionosphere [*Goertz,* 1984]. Furthermore, these waves can accelerate auroral electrons through their associated parallel electric fields [*Hasegawa,* 1976], and thus they are appealing in terms of providing a self-consistent view of the observations.

A natural question which arises is, Can FLRs produce the observed density cavities that are often associated with auroral arcs? To answer this question, we derive a model of FLRs which incorporates the nonlinear ponderomotive force (PF) of dispersive shear Alfvén waves (SAWs). It has been demonstrated that the PF of SAWs can accelerate plasma out of the topside auroral ionosphere into the equatorial magnetosphere [*Allan,* 1993; *Rankin et al.,* 1995]. Our model of FLRs is based on a dipolar topology which accounts for the inhomogeneity of plasma parameters along magnetic field lines. We discuss the derivation of the governing equations and demonstrate that the combination of the PF and dispersive effects in dipolar FLRs can give a unified view of many observational features, including the relationship between the azimuthal magnetic and radial electric fields, density cavity formation at altitudes of a few R_E, development of parallel electric fields, and the fast evolution and radial structuring of the amplitude of FLRs. For the parameters we have used, density depressions of several tens of percent are produced.

2. Reduced MHD Equations

Our model, which describes the nonlinear interaction of SAWs and density disturbances, is based on the set of reduced MHD equations that was originally derived by *Kadomtsev and Pogutse* [1974] and by *Strauss* [1976]. These authors used a one-fluid approximation with the assumption of small-perpendicular scale variations, $L_\perp/L_\parallel \ll 1$, and long time evolution, $1/\omega_{ci}t \ll 1$.

[1]On leave from the P. N. Lebedev Physics Institute, Russian Academy of Sciences, Moscow.

Paper number 1998JA900106.
0148-0227/99/1998JA900106$09.00

Here, $L_\parallel$ is the characteristic length along magnetic field lines, $L_\perp$ is the characteristic scale of perturbations in the perpendicular (radial) direction, and ω_{ci} is the ion cyclotron frequency. These equations were further elaborated by *Hasegawa and Wakatani* [1983], who included non ideal MHD effects due to electron inertia, electron pressure, and finite ion gyroradius, assuming that the electron inertia length λ_e and ion gyroradius ρ_i are small compared to the characteristic perpendicular scale: $(\lambda_e/L_\perp)^2 \sim (\rho_i/L_\perp)^2 \ll 1$. With these approximations, SAW dynamics is governed by two equations for the parallel component of the vector potential A and the scalar potential Φ:

$$\frac{\rho\mu_0}{B_0^2}\left(1+\frac{3}{4}\rho_i^2\nabla_\perp^2\right)\frac{d}{dt}\nabla_\perp^2\Phi+\nabla\cdot(\mathbf{b}\,\nabla_\perp^2 A) = \nabla_\perp\cdot\left(\frac{\mu_0}{B_0}\mathbf{b}\times\nabla_\perp P\right), \quad (1)$$

$$\frac{\partial^2 A}{\partial t^2}+\mathbf{b}\cdot\nabla\frac{\partial\Phi}{\partial t} = \lambda_e^2\frac{d}{dt}\frac{\partial}{\partial t}\nabla_\perp^2 A - \lambda_e^2(\mathbf{b}\cdot\nabla)\,V_{Te}^2\nabla\cdot(\mathbf{b}\,\nabla_\perp^2 A).$$

Here $\rho = \rho_0 + \delta\rho$ is the plasma density, B_0 is the unperturbed magnetic field, V_{Te} is the electron thermal velocity, $P = P_0 + \delta P$ is the plasma pressure, and $\mathbf{b}$ is the unit vector in the direction of the total magnetic field. SAW coupling to density and pressure perturbations, and finite ion gyroradius effects, are accounted for in the first equation (1), while the second equation accounts for electron inertia and electron thermal pressure effects. Electron inertia dominates in the low-beta limit, $\beta < m_e/m_i$, while electron pressure effects are more important in higher beta plasmas [*Hasegawa,* 1976; *Goertz,* 1984]. According to the recent analysis by *Lysak and Lotko* [1996], this approximation also provides a reasonably good description of electron kinetic effects in the intermediate regime $\beta \sim m_e/m_i$, for which the SAW phase velocity is comparable to the electron thermal velocity. This is true, provided we remain in the regime of weak dispersion, $\lambda_e \ll L_\perp$.

Plasma dynamics along magnetic field lines is accounted for by the pair of hydrodynamic equations:

$$\rho\frac{dV_\parallel}{dt} = -\mathbf{b}\cdot\nabla P+\frac{\rho}{B_0^2}\nabla_\perp A\cdot\frac{d}{dt}\nabla_\perp\Phi + \frac{1}{B_0}\nabla_\perp A\times\nabla_\perp P, \quad (2)$$

$$\frac{1}{\rho}\frac{d\rho}{dt} = \frac{1}{B_0}\frac{\partial}{\partial t}\delta B_\parallel-\nabla\cdot(\mathbf{b}\,V_\parallel),$$

describing the parallel component of the ion fluid velocity $V_\parallel$, ion density, and compressional perturbation of the magnetic field $\delta B_\parallel$. According to Ampere's law, $\delta B_\parallel$ is associated with perturbations of the plasma pressure:

$$\nabla_\perp\delta B_\parallel = -\frac{\mu_0}{B_0}\nabla_\perp P-\frac{\mu_0\rho}{B_0^2}\mathbf{b}\times\frac{d}{dt}\nabla_\perp\Phi. \quad (3)$$

The second term on the right hand side of the first equation (2) describes the excitation of ion acoustic waves (IAWs) by the SAW ponderomotive force. The derivation of the full set of reduced equations (1) - (3) has been presented recently by *Frycz et al.* [1998].

3. Nonlinear Shear Alfvén Waves in a Dipolar Magnetosphere

We now apply equations (1) - (3) to the dipolar region of Earth's magnetic field, with coordinates $\mu = \cos\theta/r^2$, $\nu = \sin^2\theta/r$, ϕ representing field-aligned, radial (in the equatorial plane, EP) and azimuthal variations, respectively. Two perfectly conducting, rigid ionospheres provide reflecting boundary conditions in the μ direction and lead to the formation of standing wave fields. According to many observations of low-m ULF field line resonances in the 1–4 mHz range, we consider perturbations which depend principally on the coordinates μ and ν. The azimuthal scale length is assumed to be large, $L_\phi = 2\pi r/m \gg L_\perp$. We formally neglect all derivatives in the azimuthal direction with the exception of the ϕ component of Eq. (3). In order to describe the excitation of an FLR, we account for the compressional Alfvén wave as an external monochromatic perturbation of the parallel magnetic field and pressure with frequency ω_0 [*Rankin et al.,* 1995]: $\delta B_\parallel^{(c)} = \delta B_c\cos(\omega_0 t - m\phi)$ and $\delta P^{(c)} = \delta P_c\cos(\omega_0 t - m\phi)$. Then, (3) defines the compressional component of the electric potential Φ_c. We also assume that density perturbations are small: $|\delta\rho|/\rho_0 \ll 1$. The electric potential can then be found from the first equation (1):

$$\frac{\partial^2\Phi}{\partial t\partial\nu} = \frac{V_A^2}{h_\phi^2}\left(1-\frac{\delta\rho}{\rho_0}-\frac{3}{4}\frac{\rho_i^2}{h_\nu^2}\frac{\partial^2}{\partial\nu^2}\right)\frac{\partial h_\phi B_\phi}{\partial\mu} - (h_\nu/h_\phi)V_A^2\mathcal{B}\sin(\omega_0 t - m\phi),$$

where $B_\phi = -\partial A/h_\nu\partial\nu$ is the toroidal component of the magnetic field, $V_A = B_0/\sqrt{\rho_0\mu_0}$ is the unperturbed Alfvén velocity, and $h_\mu = h_\nu h_\phi$, $h_\phi = r\sin\theta$, $h_\nu = r^2/(\sin\theta\sqrt{1+3\cos^2\theta})$ are the metric coefficients relating the dipole coordinate system to the spherical coordinates (r,θ,ϕ). We neglect the feedback of the SAW on the fast mode and therefore we consider the driver amplitude $\mathcal{B} = m(\delta B_c + \delta P_c\mu_0/B_0)$ as a given function of μ, localized at a distance l_d near the EP: $\mathcal{B}(\mu) \propto \exp[-l^2(\mu)/l_d^2]$, where $l(\mu)$ is the position along the magnetic field line starting at the EP. Substituting the expression for Φ into the second equation in (1), we find a closed equation for the SAW mode:

$$\frac{\partial^2 h_\phi B_\phi}{\partial t^2}-\frac{1}{h_\nu^2}\frac{\partial}{\partial\mu}\frac{V_A^2}{h_\phi^2}\frac{\partial h_\phi B_\phi}{\partial\mu} = \frac{\lambda_e^2}{h_\nu^2}\frac{\partial^4 h_\phi B_\phi}{\partial t^2\partial\nu^2} - \frac{1}{h_\nu^2}\frac{\partial}{\partial\mu}\frac{V_A^2}{h_\phi^2}\left(\frac{\delta\rho}{\rho_0}+\frac{3}{4}\frac{\rho_i^2}{h_\nu^2}\frac{\partial^2}{\partial\nu^2}\right)\frac{\partial h_\phi B_\phi}{\partial\mu}-\frac{\lambda_e^2}{h_\nu^2} \quad (4)$$

$$\times\frac{\partial}{\partial\mu}\frac{V_{Te}^2}{h_\mu^2}\frac{\partial^3 h_\phi B_\phi}{\partial\mu\partial\nu^2}-\frac{1}{h_\nu^2}\frac{\partial}{\partial\mu}\frac{h_\nu}{h_\phi}V_A^2\mathcal{B}\sin(\omega_0 t - m\phi).$$

The right-hand side of this equation accounts for the effects of dispersion, density perturbations, and the compressional wave driver on SAW dynamics. These effects are assumed to produce small changes in the SAW amplitude during one period of its evolution, and therefore the SAW eigenfrequency ω_N and field-aligned eigenfunction S_N can be found by equating the left-hand side of (4) to zero:

$$-\omega_N^2 S_N = \frac{h_\phi}{h_\nu}\frac{\partial}{\partial l}V_A^2\frac{h_\nu}{h_\phi}\frac{\partial S_N}{\partial l} \tag{5}$$

where $dl = h_\mu d\mu$ is the elementary displacement along the magnetic field line. The solutions to this equation have been analyzed elsewhere [*Cummings et al.* 1969; *Taylor and Walker,* 1984; *Cheng et al.,* 1993; *Leonovich and Mazur,* 1993, 1997]. We are interested in the excitation of the principal eigenmode, $N = 1$, which is an odd function of l, with a node in the EP, $l = 0$, and maxima at the poles, $l = \pm l_{max}$. To describe the temporal and spatial evolution of the SAW amplitude, we employ an envelope approximation, $h_\phi B_\phi(\mu,\nu,\phi,t) = h_\phi^{eq}B_0^{eq}\mathrm{Re}\, b(\nu,t)\, S_1[l(\mu)]\exp i\,(m\phi-\omega_0 t)$, where h_ϕ^{eq} and B_0^{eq} are the values of corresponding quantities evaluated at the EP. This assumption is valid in a radially narrow region in the vicinity of the FLR position, where $\omega_1(\nu_0) = \omega_0$. We introduce the radial dependence of the frequency of the SAW as a linear function of the radial coordinate: $\omega_1(x) - \omega_0 \equiv \Delta\omega(x) = \omega_0 x/2l_\omega$, where l_ω is the characteristic length of the radial variation of the SAW eigenfrequency and $x = (\nu-\nu_0)L^2R_E^2$ is the radial coordinate measured with respect to the resonant magnetic shell position L in the EP. Then, the SAW amplitude is found to satisfy the following equation:

$$\frac{\partial b}{\partial t} - i\frac{\omega_0}{2}\delta\frac{\partial^2 b}{\partial x^2} = i\,(\delta\Omega - \Delta\omega)\,b + \frac{\omega_0}{2}R. \tag{6}$$

The nonlinear frequency shift $\delta\Omega$, the effective driver strength R, and the dispersion parameter δ are defined as integrals over the SAW eigenfunction:

$$\begin{aligned}
\delta\Omega &= \frac{1}{2\omega_0 L^2R_E^2}\int dl\, V_A^2\frac{h_\nu}{h_\phi}\frac{\delta\rho}{\rho_0}\left(\frac{\partial S_1}{\partial l}\right)^2,\\
R &= -\frac{1}{\omega_0^2 h_\mu^{eq}B_0^{eq}}\int dl\,\frac{h_\nu}{h_\phi}V_A^2\mathcal{B}\frac{\partial S_1}{\partial l},\\
\delta &= L^2R_E^2\left[\frac{3}{4}\int dl\,\frac{\rho_i^2V_A^2}{\omega_0^2h_\mu}\left(\frac{\partial S_1}{\partial l}\right)^2\right.\\
&\quad\left.+\int dl\,\frac{V_{Te}^2}{\omega_0^2h_\mu}\frac{\partial S_1}{\partial l}\frac{\partial S_1^2\lambda_e^2}{\partial l} - \int dl\,\frac{\lambda_e^2}{h_\mu}S_1^2\right]
\end{aligned} \tag{7}$$

where we assume the following normalization for SAW eigenfunctions: $\int dl\,(h_\nu/h_\phi)S_1^2 = L^2R_E^2$. The sign of the dispersion parameter, δ, depends on the FLR position and magnetospheric profiles. Negative δ corresponds to the dominance of electron inertia, while positive δ indicates the dominance of electron thermal pressure and ion gyroradius effects.

The nonlinear term in (6), which is proportional to $\delta\Omega$, is due to the density perturbations. Although other nonlinear effects are possible for SAWs, it was shown by *Rankin et al.,* [1995] and *Tikhonchuk et al.* [1995] that PF-driven density perturbations constitute the dominant effect for the case of standing SAWs. The equation for density perturbations follows from (2) and (3) and has the form of a driven ion acoustic wave equation

$$\left(1+\frac{C_S^2}{V_A^2}\right)\frac{\partial^2\delta P}{\partial t^2} = \frac{C_S^2}{h_\mu}\frac{\partial}{\partial l}h_\mu\left(\frac{\partial\delta P}{\partial l} - F_P\right) \tag{8}$$

where $\delta P = C_S^2\delta\rho$ is the IAW pressure, C_S is the ion sound speed, and F_P is the SAW ponderomotive force:

$$F_P = \frac{\rho_0V_\phi^2}{h_\phi}\frac{\partial h_\phi}{\partial l} - \frac{1}{h_\phi^2}\frac{\partial}{\partial l}\frac{(h_\phi B_\phi)^2}{2\mu_0} \tag{9}$$

produced by the azimuthal components of the magnetic field and flow velocity $V_\phi = (1/h_\nu B_0)\partial\Phi/\partial\nu$. Notice a component of the PF due to magnetic field line curvature (the first term on the right-hand side), which originates from the convective derivative term on the left-hand side of (2) for the parallel ion velocity.

The pressure perturbation can be expanded over IAW eigenfunctions: $\delta P = P_0^{eq}\sum_M n_M(\nu,t)U_M[l(\mu)]$ where $U_M(l)$ are the solutions to the free (without the PF) equation (8) which satisfies the boundary condition $V_\parallel = 0$ at the ionospheric ends, $l = \pm l_{max}$. The dominant IAW eigenfrequencies are smaller than the SAW eigenfrequency even if the plasma β in the EP, $\beta_{ep} = 2\mu_0P_0^{ep}/(B_0^{ep})^2$, is of the order of unity. This is due to the fact that β decreases rapidly away from the EP [*Cheng et al.,* 1993]. Then, only the time-averaged (over the period of the SAW) component of the PF is significant in (8), and the following equation describes the evolution of the amplitudes of IAW eigenmodes:

$$\frac{\partial^2 n_M}{\partial t^2} + \Omega_M^2 n_M = \frac{\omega_0^2}{2}f_M|b_1|^2, \tag{10}$$

where Ω_M is the eigenfrequency of the acoustic wave and f_M is the PF projection on the Mth IAW eigenfunction

$$\begin{aligned}
f_M &= -\frac{2(C_S^{eq})^2}{\beta_{eq}\omega_0^2L^2R_E^2}\int dl\,\frac{h_\nu}{h_\phi}\frac{\partial U_M}{\partial l}\frac{\partial S_1}{\partial l}\\
&\quad\times\left(S_1 - \frac{V_A^2}{\omega_0^2h_\phi}\frac{\partial h_\phi}{\partial l}\frac{\partial S_1}{\partial l}\right),
\end{aligned} \tag{11}$$

where we assume the following normalization for IAW eigenfunctions: $\int dl\, h_\mu U_M^2/C_S^2 = L^4R_E^4/(C_S^{eq})^2$. Since the PF is proportional to the square of the amplitude of the principal SAW eigenfunction, which is an even function of l, coupling occurs only to even acoustic modes. The nonlinear frequency shift in (6) can also be represented by an IAW harmonic expansion, $\delta\Omega = (1/2)\omega_0\sum_M n_M g_M$, with the coefficients

$$g_M = \frac{\Gamma}{\omega_0^2L^2R_E^2}\int dl\,\frac{h_\nu}{h_\phi}V_A^2U_M\left(\frac{\partial S_1}{\partial l}\right)^2 \tag{12}$$

evaluated as integrals over IAW and SAW eigenfunctions. Here, $\Gamma = P_0/\rho_0 C_S^2$ is the adiabatic constant, with the plasma pressure P_0 assumed to be constant along magnetic field lines.

The system of (6) and (10) describes the nonlinear evolution of a standing SAW that is driven by an external source. The equations are completely different from the so-called Derivative Nonlinear Schrödinger equation [*Rogister,* 1971] because they correspond to the situation where $L_\parallel \gg L_\perp$. They are also different from the nonlinear equations derived by *Hasegawa and Mima* [1976] for obliquely propagating SAWs because of our assumption of standing waves on magnetic field lines. We have solved (6) and (10) numerically with zero initial conditions for b and n_M, and with radial boundaries placed far enough away that no reflected perturbations return back to the resonance position. The particular choice of background parameters used in our calculations is discussed in the next two sections.

4. Model Parameters for the Earth's Magnetosphere

Our model (6) and (10) are similar in form to the Cartesian model developed by [*Frycz et al.,* [1998], while the coupling coefficients, R, δ, g_M, f_M, are integrals over eigenfunctions in dipolar coordinates that must be evaluated numerically. In Cartesian geometry, $f_2 = -1/(1 + C_S^2/V_A^2)$, $g_2 = -1/2$ and all other coefficients f and g are zero. In general, except for a few special cases, one can evaluate these coefficients at the resonance surface and neglect their radial dependence.

We consider analytical profiles for the plasma density and temperature in the magnetosphere that are similar to those of *Taylor and Walker* [1984 and *Streltsov and Lotko* [1997]. Taking a dipole magnetic field, $B_0 = \mathcal{M}/h_\mu$, where $\mathcal{M}$ is Earth's dipole moment, and assuming constant plasma pressure along magnetic field lines, it is found that [*Taylor and Walker,* 1984] the fundamental mode SAW eigenfrequency depends very weakly on the plasma density and temperature profiles. However, the spectrum of IAW modes is much more sensitive to the temperature profile, as are the coupling coefficients to the SAW. In our choice of plasma profiles, we are guided by the magnetospheric data analysis presented by *Streltsov and Lotko* [1997, sections 2.2, 2.3]. For the magnetic shell $L = 8$ we consider $\rho_0(\theta) = \rho_0^{eq} p(\theta)$ and $T(\theta) = T^{eq}/p(\theta)$ with the profile function $p(\theta) = [0.8 + 0.2(1 - \cos^2\theta)^{-3}]$. The plasma density in the EP, ρ_0^{eq}, is 3.34 amu, and the ion and electron temperatures at the EP correspond to $T_i^{ep} = 500$ eV and $T_e^{ep} = 150$ eV, respectively. The ratio T_i/T_e is constant along the magnetic field line. This choice of parameters corresponds to a relatively large $\beta_{eq} = 0.14$. The pressure ratio β decreases rapidly from the EP to 10^{-7} at the ionospheric ends, which coincides with a distance that is 0.2 R_E from Earth's surface, $l_{max} = 9.8 R_E$. The selected profiles of the plasma density, temperature and Alfvén velocity along the magnetic field line are shown in Figure 1. Note that the Alfvén velocity profile excludes the so-called resonator region below altitudes of approximately $1R_E$, where the velocity is observed to drop off rapidly because of increasing density. We have excluded this region because it does not change our results significantly. In particular, the eigenmode structure and frequencies of SAWs are not appreciably changed. More complicated density and temperature profiles, similar to those discussed by *Streltsov and Lotko* [1997] and *Leonovich and Mazur* [1993, 1997], will be discussed in a future publication. We should also note that during the growth phase of magnetospheric substorms, the stretched magnetic topology in the EP likely corresponds to a higher β there than we have used. However, the nonlinear effects considered here depend on averaged plasma characteristics along magnetic field lines and should not be affected strongly by magnetic field line stretching.

Using the parameters discussed above, we first determine the SAW eigenfunctions and eigenfrequencies and then evaluate the coupling coefficients according to (7). The frequency of the fundamental SAW mode is very close to that found by *Taylor and Walker* [1984] and *Cheng et al.* [1993]. It increases toward Earth with the characteristic scale length $l_\omega \approx 1R_E$. The SAW period for L shell 8 is approximately 2.7 min. To excite a SAW,

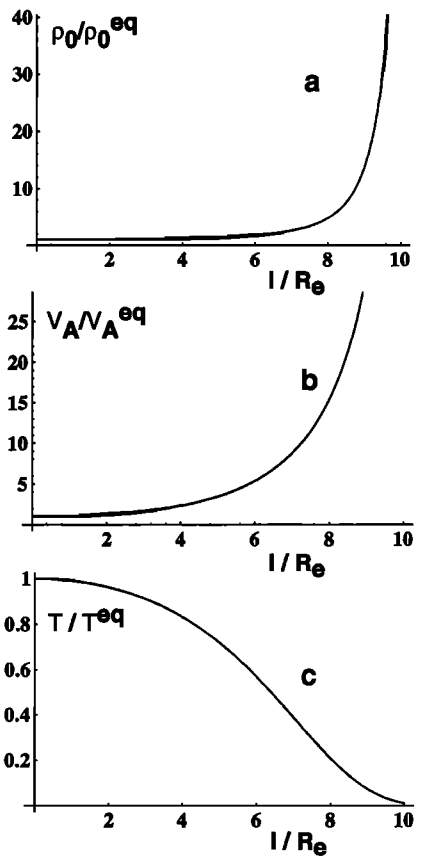

Figure 1. Profiles of (a) plasma density, (b) Alfvén velocity, and (c) temperature along the magnetic field line for the magnetic shell $L = 8$. Position $l = 0$ corresponds to the EP. All quantities are normalized to their values in the EP.

we impose a driver with amplitude $\mathcal{B}/B_0^{eq} \sim 10^{-2}$ at the EP and an exponential decay length $l_d \sim 3R_E$ (the approximate length of the field line for the $L = 8$ shell is 20 R_E). This choice corresponds to $R \approx 3 \times 10^{-3}$ and $\delta \approx 3 \times 10^{-5} R_E^2$ in (6). For this particular choice of magnetospheric parameters, the electron inertia contribution to δ is small (about 10%) and ion gyroradius and electron thermal pressure effects near the EP determine the dispersion of the fundamental SAW mode. We conclude from these estimates that nonradiative FLRs considered by *Streltsov and Lotko* [1997], which correspond to the full compensation of dispersive effects, $\delta = 0$, are very unlikely for the fundamental SAW mode, although the compensation might happen for higher SAW modes where the electron inertia contribution is more significant. The SAW eigenfunctions defining the profiles

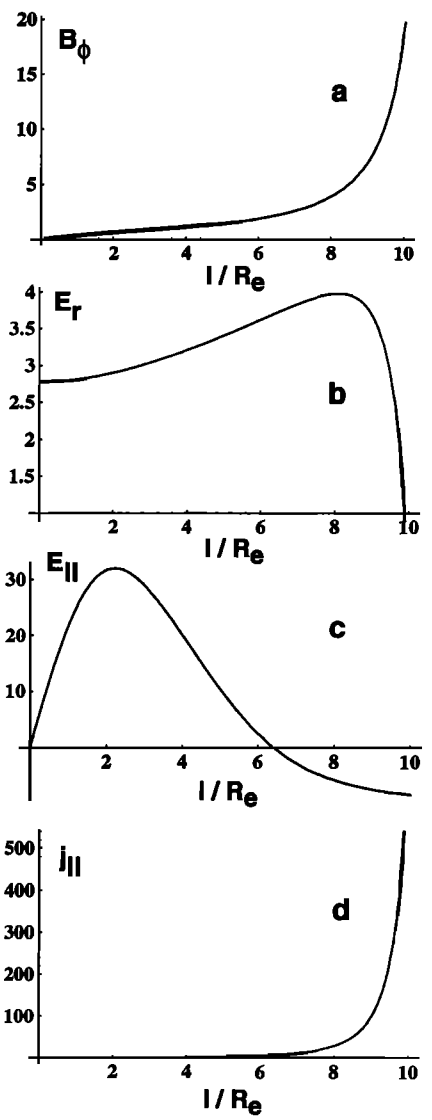

Figure 2. Profiles of the (a) azimuthal magnetic field, (b) radial electric field, (c) parallel electric field, and (d) parallel current along the magnetic field line for the magnetic shell $L = 8$. Position $l = 0$ corresponds to the EP. All quantities are normalized to their equatorial values.

of different physical parameters: $B_\phi \propto (h_\phi^{eq}/h_\phi) S_1(l)$, $E_r \propto G_\perp(l)$, $j_\parallel \propto (h_\mu^{eq}/h_\mu) S_1(l)$, and $E_\parallel \propto G_\parallel(l)$ along the magnetic field line are shown in Figure 2. Here $G_\perp(l) = LR_E(\rho_0^{eq}(h_\mu^{eq})^2 h_\phi^{eq}/\rho_0 h_\mu^2 h_\phi)\partial S_1/\partial l$ and

$$G_\parallel = \frac{\rho_0^{eq} h_\mu^{eq}}{\rho_0 h_\mu}\left[\left(\frac{V_{Te}^2}{V_A^2} - 1\right) S_1 - \frac{V_A^2}{\omega_0^2} h_\nu^2 \frac{\partial S_1}{\partial l}\frac{\partial}{\partial l}\frac{V_{Te}^2}{V_A^2 h_\nu^2}\right]$$

are the functions that describe the longitudinal structure of the radial and parallel electric fields. The azimuthal magnetic field and the parallel current have characteristic maxima near the ionospheric ends, while the radial electric field has a broad distribution with the maximum about 2 R_E above Earth's surface. The parallel electric field eigenfunction, $G_\parallel$, changes sign at $l \approx 6.5R_E$. This manifests through a change of dispersion characteristics from ion gyroradius and electron thermal effects near the EP to electron inertia closer to the ionosphere. Notice that the potential drop between the EP and the ionospheres is proportional to $H = \int_0^{l_{max}} dl\, G_\parallel(l) \approx 12.2LR_E$.

The eigenfrequencies and eigenfunctions of the IAWs are qualitatively similar to those found by *Cheng et al.* [1993], although they differ quantitatively because of different boundary conditions and a different temperature profile used in our calculations. The coupling coefficients (11) achieve a maximum around the sixth and eighth IAW modes, and the coupling coefficients (12) decrease with the IAW mode number, so we restrict our analysis to the first seven even IAW modes. Their periods, and the corresponding values of the coupling coefficients, are presented in Table 1. The IAW mode eigenfunctions are shown in Figure 3. All significant density perturbations are concentrated near the ionospheric ends at distances below 2 R_E from Earth's surface, where the temperature achieves its minimum.

5. Dissipation of SAW and IAW Modes in the Magnetosphere

We must also account for possible dissipative processes, which may compete with nonlinear terms and affect FLR dynamics. Both SAW and IAW modes have two sources of damping: volume (Landau) damping,

Table 1. Periods of Ion Acoustic Oscillations, $T_M = 2\pi/\Omega_M$, Coupling Coefficients (11) and (12), and the Coupling Parameter C_M (13) for the First Seven Even IAW Modes at the Magnetic Shell $L = 8$

Mode Number M	T_M, min	g_M	f_M	C_M
2	11.4	0.84	0.41	3.07
4	6.45	0.60	0.91	1.56
6	4.48	0.40	1.25	0.69
8	3.40	0.23	1.25	0.23
10	2.74	0.12	1.02	0.063
12	2.29	0.058	0.73	0.015
14	1.97	0.026	0.47	0.0033

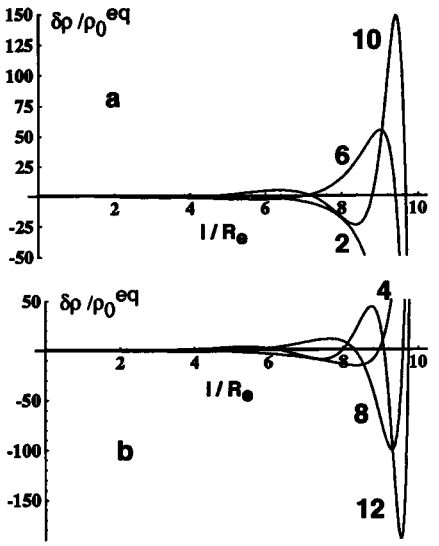

Figure 3. Profiles of plasma density perturbations in first six even IAW modes along the magnetic field line for the magnetic shell $L = 8$. Position $l = 0$ corresponds to the EP; numbers near the curves correspond the IAW eigenmode number M.

which is due to the resonance interaction of the wave with particles, and surface damping due to wave dissipation at the ionospheric boundaries. Landau damping of SAW modes is due to a resonant interaction with electrons and can be accounted for in (6) by an imaginary part of the dispersion coefficient δ. According to the recent analysis by *Lysak and Lotko* [1996], Landau damping of the fundamental SAW in the regime $(\lambda_e/L_\perp)^2 \ll 1$ is much smaller than the dispersion term and therefore does not have a significant impact on FLR dynamics. In passing, we note that the analysis by *Lysak and Lotko* [1996] refers to a box model with straight magnetic field lines; it needs further analysis relevant to a dipolar magnetic field topology where trapped particles might change significantly the SAW Landau damping. This will be considered in a future article. The remaining part of SAW damping is due to resistive losses at the ionospheric ends and results in an imaginary part of the SAW eigenfrequency, ω_1, and in the imaginary part of the frequency detuning parameter, $\Delta\omega = \omega_0 x/2l_\omega - i\gamma_1$, in (6).

According to *Taylor and Walker* [1984] and *Samson et al.* [1996], the boundary condition for (5) at $l = \pm l_{max}$ reads as: $\partial S_N/\partial l = \pm i(\omega_N/\mu_0\Sigma_P V_A^2)S_N$, where Σ_P is the height-integrated Pedersen conductivity. Assuming γ_N to be small in comparison to the SAW eigenfrequency ω_N, (5) with such a boundary condition can be solved iteratively. First, (5) is solved with the ideal boundary condition, $\partial S_N^{(0)}/\partial l = 0$ at $l = l_{max}$, resulting in a real eigenfunction, $S_N^{(0)}(l)$, and a real eigenfrequency, ω_N. In the next order, we account for the imaginary part of the eigenfrequency and solve an equation for the correction $S_N^{(1)}$:

$$2i\omega_N\gamma_N S_N^{(0)} = \omega_N^2 S_N^{(1)} + \frac{h_\phi}{h_\nu}\frac{\partial}{\partial l}V_A^2\frac{h_\nu}{h_\phi}\frac{\partial S_N^{(1)}}{\partial l}$$

with the boundary conditions $S_N^{(1)} = \partial S_N^{(1)}/\partial l = 0$ at $l = 0$. Then, applying the boundary condition at $l = l_{max}$, one finds the following expression for SAW damping:

$$\gamma_N = \frac{1}{2\mu_0\Sigma_P}\frac{\left(S_N^{(0)}\right)^2 h_\nu/h_\phi}{\int_0^{l_{max}} dl \left(S_N^{(0)}\right)^2 h_\nu/h_\phi}$$

where the numerator has to be evaluated at $l = l_{max}$. For the density profile described above and for the fundamental SAW eigenmode, this expression corresponds to the following damping time: $1/\gamma_1 \approx 5\mu_0 L R_E^2 \Sigma_P$. According to *Samson et al.* [1996], the typical value of Σ_P is ≈ 8 ohm^{-1}. For the L shell 8 this corresponds to the SAW damping time $1/\gamma_1 = 42.7$ min.

Dissipative effects are also important for IAW modes. Since the ion temperature is larger than the electron temperature, the IAW phase velocity is comparable to the thermal ion velocity. In such a plasma without a magnetic field, Landau damping of ions is comparable to the IAW frequency, and no normal modes exist. How-

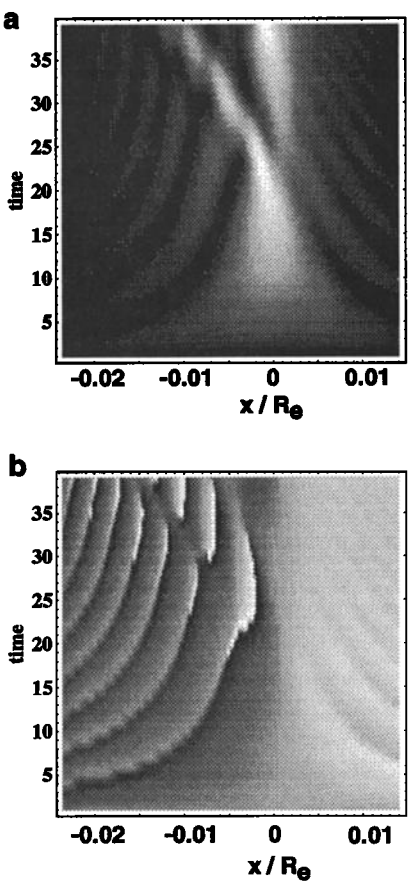

Figure 4. Radial and time dependence of the azimuthal magnetic field (a) amplitude and (b) phase in radians at an altitude of 0.5 R_E. Parameters of the model are described in the text.

ever, because of Earth's magnetic field, ions are trapped on magnetic field lines, and their bounce time is comparable to the IAW period. This might lower significantly the Landau damping coefficient. The problem of IAW damping on magnetic field lines deserves a separate study using a gyro-kinetic approach. We account for this effect in (10) in an ad hoc way by adding the term $2\Gamma_{iaw}\Omega_M \partial n_M/\partial t$ to the left-hand side of the equation, and by considering that all IAW modes have the same damping to frequency ratio, Γ_{iaw}. The results presented below correspond to relatively strong damping $\Gamma_{iaw} = 0.3$.

6. Analysis of Nonlinear Model

According to the model derived above, the sequence of physical processes is as follows [*Rankin et al.*, 1995; *Frycz et al.*, 1998]. During the initial stage of evolution, nonlinear and dispersive effects can be neglected, and the driver R in (6) causes the SAW amplitude to grow. From (7) and (10), this results in a corresponding increase in the density fluctuations and a nonlinear frequency shift $\delta\Omega$ that increases in proportion to $\delta\rho$. The latter will lead to amplitude saturation after a phase shift of $\pi/2$. This saturation is a local phenomenon for each magnetic field line, in that as an initially resonant field line moves out of resonance, an adjacent field line moves into resonance. This results in nonlinear steepening of the radial profile of the SAW amplitude and a shift of the original FLR position toward Earth in the EP or equatorward when observed at the ionosphere.

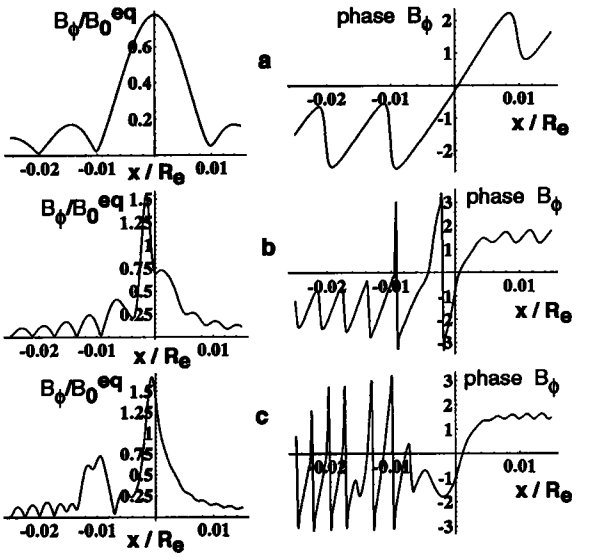

Figure 6. Radial distribution of the azimuthal magnetic field amplitude (left column) and phase (right column) at an altitude 0.5 R_E, for times corresponding to t = (a) 10, (b) 25, and (c) 40 SAW periods. Parameters of the model are described in the text. The magnetic field amplitude is normalized by the equatorial magnetic field $B_0^{eq} = 60$ nT.

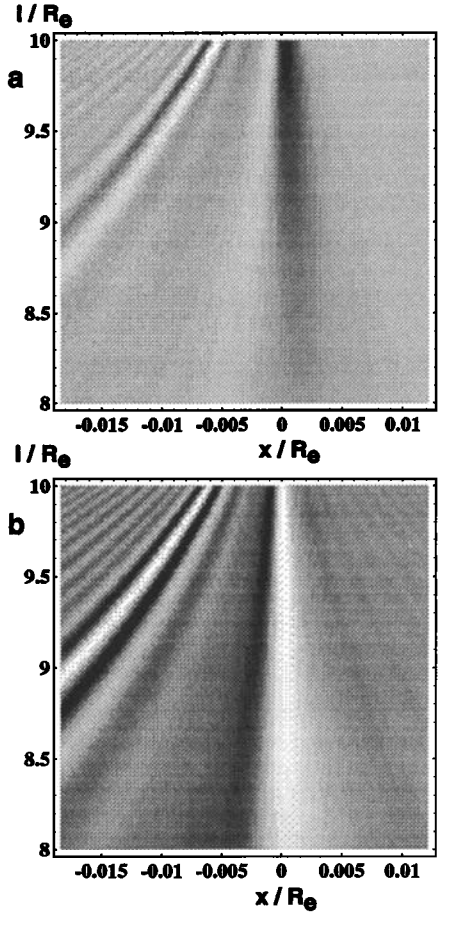

Figure 5. Radial and longitudinal dependence of the (a) azimuthal magnetic field and the (b) parallel electric field at time of 40 SAW periods. Parameters of the model are described in the text.

Nonlinear PF steepening of the amplitude of the FLR eventually causes dispersive effects to come into play and leads to a radially directed energy flux out of the resonance region. The direction of the energy flux is determined by the sign of the dispersion parameter δ in (7). The last term in the expression for δ corresponds to electron inertia dispersion and leads to Airy-like solutions with fields propagating Earthward of the resonant field line (or equatorward near the polar ionospheres). The first two terms are due to finite ion gyroradius and electron thermal pressure effects, respectively. If these terms dominate, they give wave fields propagating poleward of the initially resonant field line near the ionospheres. Notice that in this regime, dispersion and nonlinearity act in opposite directions, in contrast to the electron inertia case. This leads to different behavior in the nonlinear dynamics, where soliton formation becomes possible in the former case.

The relative importance of different processes and the characteristic times of FLR evolution can be estimated using (6) and (10). We first neglect the dispersion term and assume that the time of nonlinear saturation is larger than the IAW period. Then, estimating the amplitudes of IAW modes from (10), and comparing the nonlinear, nonstationary, and driver terms in (6), one finds the amplitudes of the principal SAW and IAW

modes and the characteristic time of nonlinear saturation:

$$b_{nl} = \left(\frac{R}{C}\right)^{1/3}, \; t_{nl} = \frac{2}{\omega_0}(R^2C)^{-1/3},$$
$$n_{Mnl} = \frac{C_M}{g_M}\left(\frac{R}{C}\right)^{2/3} \tag{13}$$

where $C = \sum_M C_M \approx 5.63$ for the chosen parameters, $C_M = g_M f_M \omega_0^2/2\Omega_M^2$, and the summation extends over all even M. In the opposite limit, where nonlinear effects can be ignored, Eq. (6) gives the time, amplitude, and the spatial scale of linear dispersive saturation,

$$b_l = R\left(\frac{l_\omega^2}{|\delta|}\right)^{1/3}, \; t_l = \frac{2}{\omega_0}\left(\frac{l_\omega^2}{|\delta|}\right)^{1/3}, \; l_l = (|\delta| l_\omega)^{1/3}.$$

Finally, ionospheric dissipation results in linear FLR saturation on the timescale $t_{dis} \approx 1/\gamma_1$. For the magnetospheric parameters chosen in the previous section, $(R^2C)^{1/3} > 2\gamma_1/\omega_0$, $(\delta/l_\omega^2)^{1/3}$, and therefore nonlinear effects occur on a faster timescale and dominate the resulting FLR evolution.

In the following figures, we discuss the temporal evolution and spatial distribution of fields in the vicinity of the linear FLR region. Along with the azimuthal magnetic field and plasma density, we show the radial electric field,

$$E_r = B_0^{eq}\frac{(V_A^{eq})^2}{\omega_0 L R_E}\,\mathrm{Im}\, b\, G_\perp(l)\, \exp i(m\phi - \omega_0 t),$$

the parallel electric field,

$$E_\parallel = -\omega_0(\lambda_e^{eq})^2 B_0^{eq}\,\mathrm{Im}\,\frac{\partial b}{\partial x}\, G_\parallel(l)\, \exp i(m\phi - \omega_0 t),$$

and the parallel component of the electric current,

$$j_\parallel = \frac{B_0^{eq}}{\mu_0}\frac{h_\mu^{eq}}{h_\mu}\mathrm{Re}\frac{\partial b}{\partial x}\, S_1(l)\, \exp i(m\phi - \omega_0 t).$$

In Figure 4, we show the radial distribution of the SAW amplitude $|b|$ and phase -Arg(b) and their evolution in time near the ionosphere where B_ϕ achieves its maximum (cf. Figure 2a). Nonlinear saturation first occurs at 10 - 15 SAW periods, following the time at which the driver is switched on. The resonance narrows, and eventually, dispersion effects manifest and transfer energy away from the resonance. The partial compensation of nonlinear and dispersive effects (dominated by gyro and electron thermal effects) results in the formation of a soliton structure which propagates with almost constant velocity in the poleward direction. The detailed physics of soliton formation and its subsequent dynamics have been discussed elsewhere [*Frycz et al.*, 1998]. A new structure subsequently appears near the original FLR position, and the process of soliton emission repeats with a characteristic timescale of 20 SAW periods. This timescale is larger than the characteristic period of the dominant IAW mode.

The radial structure of the FLR is demonstrated in Figure 5 for a time equal to 40 SAW periods and for altitudes varying from 2 R_E down to the height of the ionosphere. The narrowing and convergence of the magnetic field (Figure 5a) and the parallel electric field (Figure 5b) is due to the convergence of Earth's dipolar magnetic field. Note that the maximum amplitude of the parallel electric field is outside of the exact FLR position where the azimuthal magnetic field achieves its maximum. This can also be seen in Figure 6, which shows the radial distribution of the amplitude and phase of the SAW magnetic field at three different times, and for an altitude that is 0.5 R_E above Earth. The radial width of solitons in Figure 6c is roughly 10 km. Although this width is defined by ion gyroradius and electron thermal pressure dispersion, it is comparable to the electron inertial length near the ionosphere.

The radial distribution of the parallel electric field is illustrated in Figure 7 for distances of 2.5 R_E and 9.5 R_E from the EP at a time equal to 40 SAW periods. The parallel electric field exhibits narrower structures than the azimuthal magnetic field since it is proportional to the radial derivative of the magnetic field amplitude. The maximum amplitude of the parallel electric field is about 0.5 μV/m near the EP and approximately 2-3 times less at the ionosphere. It is not evident that such a field can directly accelerate particles which can excite optical auroral emissions. There are two reasons for this. First, the large-amplitude part of $E_\parallel$ is localized to high altitudes, where the plasma concentration is low. Second, the full potential drop between the EP and the ionosphere, $\Phi_\parallel = \int_0^{l_{max}} E_\parallel dl$, is less than 20 V for the model parameters chosen in our example. This is obviously smaller than the 500 – 1000 V values that are typical of many auroral arcs. However, we have chosen modest parameters that illustrate typical behavior

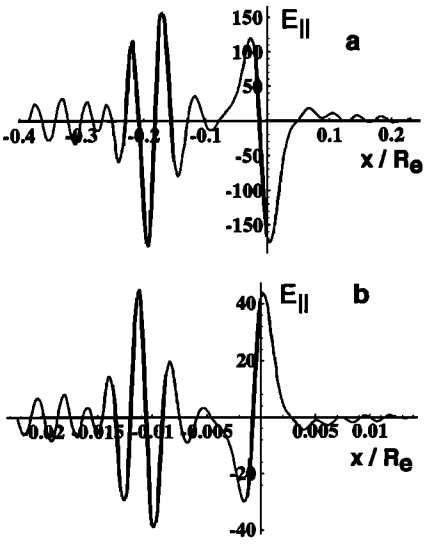

Figure 7. Radial distribution of the parallel electric field at an altitude (a) 7.5 R_E and (b) 0.5 R_E for time t = 40 SAW periods. Parameters of the model are described in the text. The electric field is normalized by $\omega_0(\lambda_e^{eq})^2 B_0^{eq}/R_E = 0.005\,\mu$V/m.

predicted by our model. In particular, the driver R in our model equations gives a saturated SAW magnetic field of 60 nT at the ionosphere, which is much smaller than observed values of a few hundred nanoteslas. With a larger amplitude driver, we obtain considerably larger potentials (up to an order of magnitude increase) and a much faster evolution of nonlinear effects. Different magnetospheric profiles of density, temperature, and the ratio of T_e to T_i will also lead to different results, although we stress that our chosen parameters are representative of real magnetospheric values. The radial distribution of the potential drop is shown in Figure 8. The radial width of the potential peaks is about 10 km, and the maximum amplitude is about 15 - 20 V.

The phase structure of the azimuthal SAW magnetic field also contains important information. It is evident from Figure 4 that soliton generation is accompanied by a 2π phase shift, which is manifested by a discontinuity of lines where the phase acquires a 2π phase jump. This effect is even more evident in Figure 6. In the period of linear evolution, there is a clear phase shift from $-\pi/2$ to $\pi/2$ across the resonance, which provides well-accepted evidence for identifying FLRs. However, during later times, the phase profile is substantially altered. Although a phase shift of π is still evident near the resonance position, there are additional 2π phase shifts as one crosses the soliton locations. Observational signatures of such additional phase shifts might be considered as a confirmation of nonlinear FLR saturation.

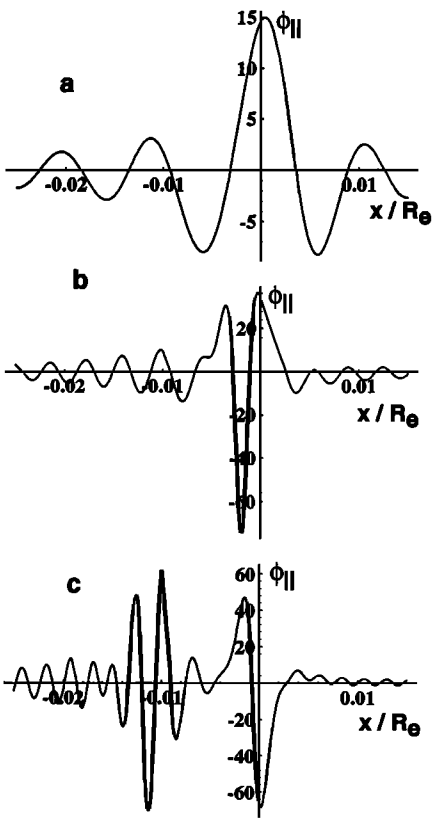

Figure 8. Radial dependence of the parallel potential drop, $\phi_{||} = \int E_{||} dl$, between the EP and Earth's surface at three times corresponding to t = (a) 10, (b) 25, and (c) 40 SAW periods. Parameters of the model are described in the text. The potential amplitude is normalized by $\omega_0 L(\lambda_e^{eq})^2 B_0^{eq} = 0.26$ V.

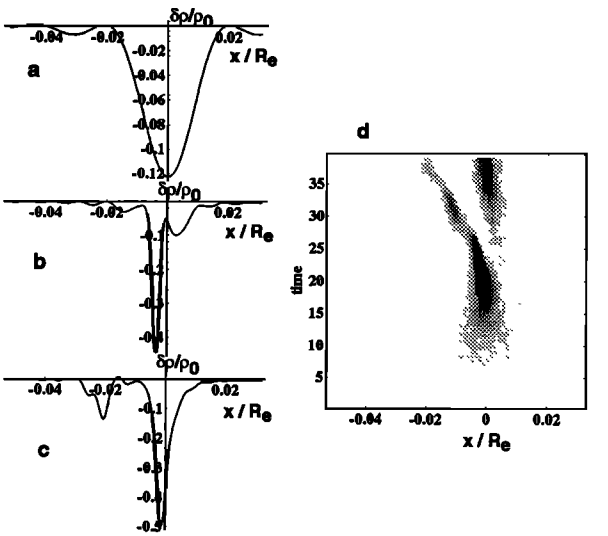

Figure 9. Radial dependence of the density perturbation, $\delta\rho/\rho_0$, at the altitude 1.5 R_E from Earth's surface at times corresponding to t = (a) 10, (b) 25, and (c) 40 SAW periods. Figure 9d represents the radial and time dependence of the density perturbation, $\delta\rho/\rho_0^{eq}$, at the same altitude. Parameters of the model are described in the text.

Nonlinear saturation of FLRs is associated with the excitation of large-amplitude density perturbations by the PF of SAWs. The temporal evolution of density perturbations $\delta\rho/\rho_0^{eq}$ is shown in Figure 9 for an altitude of 1.5 R_E above Earth and in Figure 10 for an altitude of 0.5 R_E. The radial structuring of the plasma density is very similar to that of the azimuthal magnetic field (cf. Figure 4), namely, soliton formation manifests itself in a deep narrow density depletion which moves northward with the soliton. The width of the density cavity decreases with altitude from 60 km at an altitude of 1.5 R_E to less than 10 km at an altitude of 0.5 R_E. The altitude dependence of the density cavities can be seen in Figure 11 for three consecutive time moments corresponding to 10, 25, and 40 SAW periods. The depth of the density cavities increases with time and achieves a magnitude of approximately 50 – 70% at a time around 40 SAW periods. The longitudinal distribution of density perturbations is shown in Figure 12 for the resonance magnetic field line, $x = 0$, for eight consecutive moments of time, each five SAW periods apart. The density perturbation is positive near the EP and negative at the ionospheric ends. Its magnitude gradually increases during the first 20 SAW periods, then drops during the period of soliton emission from the resonance, and then increases with time again. The time of about 20 SAW periods characterizes the periodicity of IAW density perturbations in the FLR region.

Finally, we comment on the harmonic composition of the plasma density perturbation. Although we account

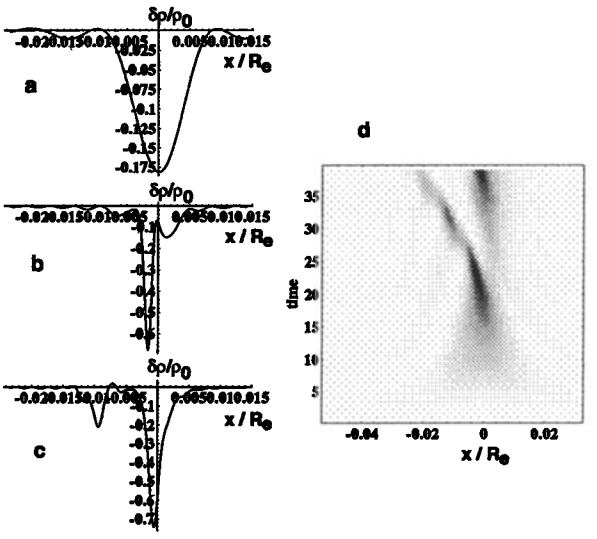

Figure 10. Radial dependence of the density perturbation $\delta\rho/\rho_0$ at the altitude 0.5 R_E from Earth's surface at times corresponding to t = (a) 10, (b) 25, and (c)40 SAW periods. Figure 10d represents the radial and time dependence of the density perturbation, $\delta\rho/\rho_0^{eq}$, at the same altitude. Parameters of the model are described in the text.

in this example for seven even IAW modes, it has been verified that the fundamental mode, $M = 2$, dominates the plasma response. This is illustrated in Figure 13, where the radial profile of density perturbations consisting of seven IAW modes (solid lines) is compared with the mode $M = 2$ contribution (gray lines). One can see that the overall contribution of higher modes is less than 20%. This occurs because the Mth mode contribution to the nonlinear frequency shift, according to (13), is proportional to the parameter $C_M = g_M f_M \omega_0^2/2\Omega_M^2$, which decreases dramatically with mode number (cf. Table 1).

The formation of density cavities by the ponderomotive force at the nonlinear stage of FLR evolution is one of the most prominent manifestations of our model. Therefore recent observations of density cavities by *Lundin et al.* [1994] and *Stasiewicz et al.* [1997] could be considered as an indication of the validity of our model. More recently, in yet to be published work, W. Lotko and J. C. Samson (private communication, 1998) have reported simultaneous CANOPUS [*Rostoker et al.*, 1994] and FAST [*Carlson et al.*, 1998] satellite observations of magnetospheric density cavities in association with FLRs. Their observations confirm the colocation of magnetic signatures on the ground with satellite measurements of azimuthal magnetic fields, parallel electric fields, and precipitating electron and ion beams. These effects are all predicted self-consistently by our nonlinear model of FLRs.

7. Conclusions

We have presented a theory of dispersive shear Alfvén waves on dipole magnetic field lines in Earth's magnetosphere. The theory describes coupling between SAWs and a spectrum of ion acoustic waves that is excited by the ponderomotive pressure of SAWs. Results are shown for fundamental mode SAWs, since these modes are often observed on the ground. However, higher harmonics should produce stronger nonlinear effects that might be more easily observed during in situ probing of the magnetosphere. One explanation for why high harmonics are not often seen in ground observations is that they are being refracted by the ionosphere. For modest model parameters, we find that the PF can drive radially localized density cavities at altitudes below 2-3 R_E on field lines that map to 8 R_E in the EP. The characteristics of these density cavities are in good agreement with satellite observations of such structures in the auroral magnetosphere. Simultaneous measurements of the density cavities, azimuthal magnetic fields, radial electric fields, parallel currents, and parallel electric fields could provide an important insight into mechanisms of auroral activity in the polar ionosphere.

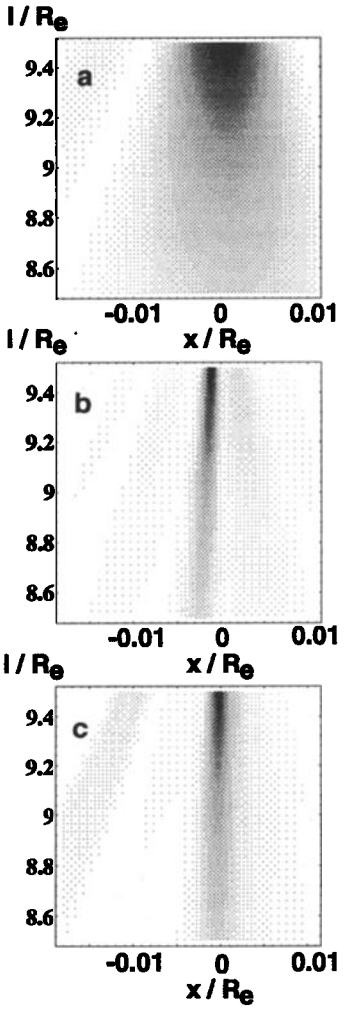

Figure 11. Radial and altitude dependence of the density perturbation, $\delta\rho/\rho_0^{eq}$, at time moments t = (a)10, (b) 25, (c) 40 SAW periods. Parameters of the model are described in the text.

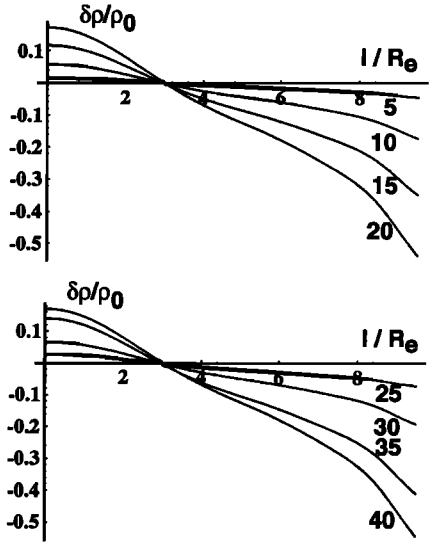

Figure 12. Dependence of the relative density perturbation, $\delta\rho/\rho_0$, on the altitude along the magnetic field line; $l = 0$ corresponds to the EP. Numbers near the curves indicate time in SAW periods. Parameters of the model are described in the text.

In the particular example discussed in this paper, the parallel potential drop is to too small to explain the acceleration of particles to energies that can excite optical aurora. However, this is a direct consequence of the strength of the compressional driver in our nonlinear model and in our initial assumption concerning the relation between the ion and electron temperatures, $T_i/T_e = 3.3$. Lower ratio T_i/T_e will significantly enhance the parallel electric field and the parallel potential drop. The richness of the physics associated with standing SAWs in Earth's magnetosphere obviously demands further investigation and may go some way to explaining observations of modulated auroral arcs and simultaneous large-amplitude density depletions. In a future publication we will present a detailed parametric study of the predictions of our model under varying ambient magnetospheric conditions. This will provide definitive predictions concerning the behavior of temporally modulated auroral arcs that are often observed in the auroral zone.

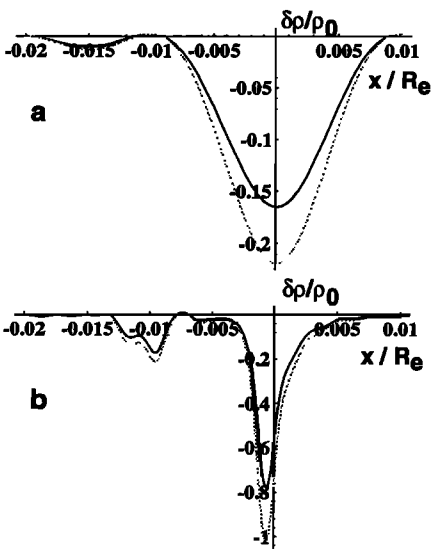

Figure 13. Radial dependence of the density perturbation, $\delta\rho/\rho_0$, at an altitude 0.5 R_E from Earth's surface at time corresponding to $t =$ (a) 10 and (b) 40 SAW periods. Parameters of the model are described in the text. The solid line corresponds to results accounting for seven IAW modes, while the gray line demonstrates the contribution of only the lowest mode $M = 2$.

Acknowledgments. Research for this project has been supported by the Canadian Space Agency, the Natural Science and Engineering Research Council of Canada, NSERC, and the Russian Foundation for Basic Research.

The Editor thanks both of the referees for their assistance in evaluating this paper.

References

Allan, W., Plasma energization by the ponderomotive force of magnetospheric standing Alfvén waves, *J. Geophys. Res., 98,* 11,383, 1993.

Carlson, C. W., R. F. Pfaff, and J. G. Watzin, The Fast Auroral Snapshot (FAST) mission, *Geophys. Res. Lett., 25,* 2013, 1998.

Cheng, C. Z., T. C. Chang, C. A. Lin, and W. H. Tsai, Magnetohydrodynamic theory of field line resonances in magnetosphere, *J. Geophys. Res., 98,* 11,339, 1993.

Cummings, W. D., R. J. O'Sullivan, and P. J. Coleman Jr., Standing Alfvén waves in the magnetosphere, *J. Geophys. Res., 74,* 778, 1969.

Frycz, P., R. Rankin, J. C. Samson, and V. T. Tikhonchuk, Nonlinear field line resonances: Dispersive effects, *Phys. Plasmas, 5,* 3565, 1998.

Goertz, C. K., Kinetic Alfvén waves on auroral field lines, *Planet. Space Sci., 32,* 1387, 1984.

Hasegawa, A., Particle acceleration by MHD surface wave and formation of aurora, *J. Geophys. Res., 81,* 5083, 1976.

Hasegawa, A., and K. Mima, Exact solitary Alfvén wave, *Phys. Rev. Lett., 37,* 690, 1976.

Hasegawa, A., and M. Wakatani, Finite-larmor-radius magnetohydrodynamics equations for microturbulence, *Phys. Fluids, 26,* 2770, 1983.

Kadomtsev, B. B., and O. P. Pogutse, Nonlinear helical perturbations of a plasma in the tokamak, *Sov. Phys. JETP, 38,* 283, 1974.

Leonovich, A. S., and V. A. Mazur, A theory of transverse small-scale standing Alfén waves in an axially symmetric magnetosphere, *Planet. Space. Sci., 41,* 697, 1993.

Leonovich, A. S., and V. A. Mazur, A model equation for monochromatic standing Alfén waves in the axially symmetric magnetosphere, *J. Geophys. Res., 102,* 11443, 1997.

Lundin, R., L. Eliasson, G. Haerendel, M. Boehm, and B. Holback, Large scale auroral density cavities observed by Freja, *Geophys. Res. Lett., 21,* 1903, 1994.

Lysak, R. L., and W. Lotko, On the kinetic dispersion relation for shear Alfvén waves, *J. Geophys. Res., 101,* 5085, 1996.

Persoon, M., D. A. Gurnett, W. K. Peterson, J. H. Waite Jr., J. L. Burch, and J. L. Green, Electron density depletions in the nightside auroral zone, *J. Geophys. Res., 93,* 1871, 1988.

Rankin, R., P. Frycz, V. T. Tikhonchuk, and J. C. Samson, Ponderomotive saturation of magnetospheric field line resonances, *Geophys. Res. Lett., 22,* 1741, 1995.

Rogister, Parallel propagation of nonlinear low-frequency waves in high-β plasma, *Phys. Fluids, 14,* 2733, 1971.

Rostoker, G., J. C. Samson, F. Creutzberg, T. J. Hughes, D. R. McDiarmid, A. G. McNamara, A. Vallance Jones, D. D. Wallis and L. L. Cogger, CANOPUS–A ground based instrument array for remote sensing in the high latitude ionosphere during ISTP/GGS program, *Space Sci. Rev., 71,* 743, 1994.

Samson, J. C., L. L. Cogger, and Q. Pao, Observations of field line resonances, auroral arcs, and auroral vortex structures, *J. Geophys. Res., 101,* 17,373, 1996.

Stasiewicz, K., G. Gustafsson, G. Marklund, P.-A. Lindqvist, J. Clemmons, and L. Zanetti, Cavity resonators and Alfvén resonance cones observed on Freja, *J. Geophys. Res., 102,* 2565, 1997.

Strauss, H. R., Nonlinear three-dimensional magnetohydrodynamics of noncircular tokamaks, *Phys. Fluids, 19,* 134, 1976.

Streltsov, A. V., and W. Lotko, Dispersive, nonradiative field line resonances in a dipolar magnetic field geometry, *J. Geophys. Res., 102,* 27,121, 1997.

Taylor, J. P. H. and A. D. M. Walker, Accurate approximate formulae for toroidal standing hydromagnetic oscillations in a dipolar geomagnetic field, *Planet. Space Sci., 32,* 1119, 1984.

Tikhonchuk, V. T., R. Rankin, P. Frycz, and J. C. Samson, Nonlinear dynamics of standing shear Alfvén waves, *Phys. Plasmas, 2,* 501, 1995.

Trondsen, T. S., L. L. Cogger, and J. C. Samson, Observations of asymmetric, multiple auroral arcs. *Geophys. Res. Lett., 24,* 2945, 1997.

Wei, C. Q., J. C. Samson, R. Rankin, and P. Frycz. Electron inertial effects on geomagnetic field line resonances. *J. Geophys. Res., 99,* 11,265, 1994.

R. Rankin, J. C. Samson, and I. Voronkov, Department of Physics, University of Alberta, Edmonton,T6G 2J1, Canada. (rankin@space.ualberta.ca)

V. T. Tikhonchuk, P. N. Lebedev Physics Institute, Russian Academy of Sciences, Moscow, 117924, Russia.

(Received September 1, 1998; revised October 2, 1998; accepted November 3, 1998.)